ELSEVIER

Journal of Non-Crystalline Solids 285 (2001) 181–186

JOURNAL OF NON-CRYSTALLINE SOLIDS

www.elsevier.com/locate/jnoncrysol

Small angle neutron scattering characterization of colloidal and fractal aerogels

Richard F. Reidy [a,*], Andrew J. Allen [b], Susan Krueger [b]

[a] *Department of Materials Science, University of North Texas, Denton TX 76203-5310, USA*

[b] *Materials Science and Engineering Laboratory, National Institute of Standards and Technology, Gaithersburg, MD 20899, USA*

Abstract

Extreme length scales of aerogel structures limit the effectiveness of many characterization techniques. With the resolutions commensurate with the length scales found in these materials, small angle neutron scattering measurements were conducted and interpreted using several models developed for other ceramic systems (polydispersed hard-sphere, fractal, and maximum entropy models). Interference (polydispersed hard-sphere) and maximum entropy models indicate that tetraethoxysilane (TEOS) aerogel structure may be comprised of oblate nanoparticles within oblate mesoparticles. The fractal model was used to describe the structures of triethoxysilane (TES) and trimethoxysilane (TMS) aerogels and to quantify their fractal properties. TES aerogels appear to be networks of volume fractals while TMS aerogels contain both volume and surface fractal elements.

PACS: 41.12.Fx

1. Introduction

Small angle neutron scattering (SANS) is a well-recognized investigative method to characterize material microstructure [1]. Many research efforts have employed SANS and small angle X-ray scattering (SAXS) to characterize aerogel structures by applying these techniques to examine fractal behavior at specific length scales and to study changes in structure with respect to processing variables [2–7]. A comprehensive method to describe structure using small angle scattering has been put forth by Beaucage [8,9]. In this Unified Method, different structural levels (regions of Q-space) are fitted with Guinier and power law terms. Instead of using power law fits, this study examines the viability of modeling SANS of aerogels with a single physical model across the entire Q-range. Additionally, a maximum entropy model has been fitted to the high Q (small length scale) region. Previously, these models have been employed to study a variety of material systems including clays, concrete, and nano-structured ceramics [10–12]. Three aerogel systems were selected commensurate with the capabilities of each model. While the models differ, each attempts to characterize the size and shape of a meso-sized moeity (particles >2.5 nm) and the void space within and between these moeities.

Although the distinctions are subject to debate, one can separate aerogels into two different types

* Corresponding author: Tel.: +1-940 369 7115; fax: +1-940 565 4824.

E-mail address: reidy@unt.edu (R.F. Reidy).

0022-3093/01/$ - see front matter
PII: S0022-3093(01)00451-3

of structures: colloidal (or particle-like) and fractal (or networked). Base-catalyzed tetraethoxysilane (TEOS) was chosen as a representative colloidal system, and neutral-catalyzed triethoxysilane (TES) and trimethoxysilane (TMS) were chosen as fractal aerogels. These structural distinctions have been imposed for this paper but the authors do not contend that colloidal aerogels are bereft of fractal character.

2. Experimental

2.1. Sample preparation

Aerogels were synthesized from TES, TMS, and TEOS, as described in Table 1, forming gels in 1 cm diameter vials at 23°C. The samples were aged in solvent for three days and supercritically dried in liquid CO_2. The physical and neutron transmission characteristics of the dried aerogel disks are noted in Table 2. The transmission coefficient was calculated as the ratio of sample transmission and empty beam transmission. The errors noted are standard deviations.

2.2. Small angle neutron scattering

Experiments were conducted on the 30 m SANS instrument on neutron guide NG-7 at the NIST Center for Neutron Research. Detector distances of 1.2, 4 and 15.3 m were used to effectively examine a large range of length scales, and 5 Å neutrons were employed to resolve extremely small length scales.

Three models were chosen to characterize these data: interference, maximum entropy and Guinier Fractal methods. Described in the work of Allen et al. the interference model assumed a lognormal size distribution of spheroidal scatterers with nine possible preset aspect ratios, β [10]. The small-angle scattering cross-section was assumed as

$$d\Sigma/d\Omega = n_o P(Q) S_1(Q) + \mathrm{BGD} + P_{\mathrm{add}}, \quad (1)$$

where n_o is the pore number/sample volume (lognormal number size distribution), BGD describes scattering from a flat incoherent background and P_{add} is an additional Porod scattering term. In this effort, $P_{\mathrm{add}} = 0$. $P(Q)$ is the scattering form factor of a single particle or pore, and is equal to the square of the scattering amplitude, $|F(Q)|$, for a spheroidal pore averaged over all orientations and over an assumed lognormal size distribution.

$$P(Q) = \langle |F(Q)|^2 \rangle. \quad (2)$$

$S_1(Q)$ is an effective modified structure factor incorporating interference effects and is given by

$$S_1(Q) = 1 + B(Q)[S(Q) - 1]. \quad (3)$$

$B(Q)$ is the ratio of two different orientational averages of the scattering amplitude to permit polydispersity of particle size and shape.

$$B(Q) = |\langle F(Q) \rangle|^2 / \langle |F(Q)|^2 \rangle. \quad (4)$$

$S(Q)$ is the interference structure factor for an orientationally random distribution of nearest neighbor scatterers, based on a Percus–Yevick hard sphere model [13,14]. Two important parameters

Table 1
Aerogel synthesis conditions

Sample	Solvent, solvent/alkoxide ratio	Catalyst, water/alkoxide ratio
TEOS	Ethanol, 4	0.01N NH_4OH (pH = 9.6), 4
TES (TE1, TE2)	Ethanol, 4	H_2O (pH = 5), 3
TMS	Methanol, 4	H_2O (pH = 5), 3

Table 2
Sample size and neutron transmission coefficient (errors are in standard deviations)

Sample	Sample thickness (±0.005 cm)	Sample density ($g/cm^3 \pm 0.0005$)	Transmission coefficient (sample/empty beam)
TEOS	0.62	0.367	0.766 (±0.0002)
TES (TE1, TE2)	0.20, 0.40	0.188, 0.188	0.984, 0.916 (±0.0002)
TMS	0.17	0.263	0.984 (±0.0002)

are included in this term: η, the local volume fraction, and D_{int}, the mean distance between spheroidal scatterers. This model also predicts particle size and volume fraction of scatterers.

The maximum entropy model does not fit empirical distribution models, but derives a particle size distribution consistent with the maximum configurational entropy (hence the least structure) [1]. This method was used to characterize the high Q region (small length scales) of the SANS profile. The particle size distributions were determined using methods developed by Potton et al. [15]. The necessary input parameters are an assumed particle shape and the contrast (square of the scattering length density) of the fundamental scattering moeity. Optimal fits are determined by changing particle aspect ratios. Details of the maximum entropy model and its algorithm are explained in the appendix of [1].

In the fractal model, the small-angle scattering cross-section is separated into four components terms: volume fractal, surface fractal, single globule and flat background scattering. Several terms are included in the volume or mass-fractal component: ϕ, the volume fraction of scatterers, D_v, the volume or mass fractal dimension, ξ_v, the volume or mass fractal correlation length, R_o, the mean radius of the volume fractal building block, and β, the aspect ratio of the building block. Two additional terms, η, the local volume fraction and R_c, the correlation hole radius, are sensitive to nearest and next nearest neighbor globules and are necessary to create a smooth fit. The volume fractal dimension, D_v, varies from 1 to 3 (usually 2 to 3) and, for a uniformly random structure, $D_v = 3$. The volume fractal correlation length, ξ_v, defines the average upper-limit length-scale for the volume-fractal domain.

The surface fractal component is defined by D_s, the surface fractal dimension ($2 < D_s < 3$ for non-smooth surfaces), ξ_s, the surface fractal correlation length, S_o, and the apparent surface area for length scale, ξ_s. The total surface in the surface fractal component, S_{SF}, is described as

$$S_{SF} = S_o(\xi_s/R_c)^{Ds-2}. \quad (5)$$

Detailed discussions of these components can be found in references [11,12,16].

3. Results

SANS experiments were conducted on TEOS, TES, and TMS samples, and each system exhibited different scattering behavior (Fig. 1). The TEOS data clearly show an interference peak while the TMS and TES results exhibit distinctly fractal behavior. The interference model of TEOS results indicates that this aerogel is made up of loosely packed flattened (oblate) globules with an average separation distance of approximately 230 Å (Fig. 2). The disk-like globules have an aspect ratio of 1/5 and radii of approximately 70 Å. The oblate globules are mostly void space (local packing fraction) only 8% solid structure. Maximum entropy analyses (Fig. 3) suggest that the 'building blocks' of the larger globules (described by the interference model) are slightly oblate structures with an aspect ratio of 1/3 with diameters of 10, 23, and 37 Å.

SANS results from TES and TMS samples were modeled using a fractal approach [11,12]. The model provides fractal descriptions of the material microstructure and structural parameters of the aerogel (e.g., surface and mass fractal dimensions and domains, packing fractions). If, through observation or repeated trials, surface fractal

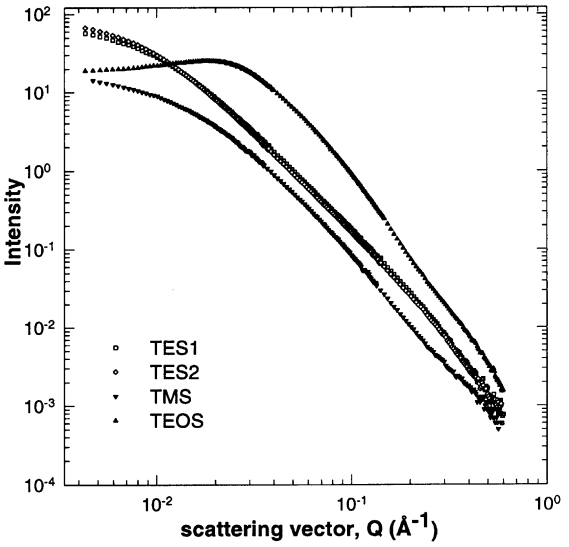

Fig. 1. Fig. 1 SANS results for TEOS, TES, and TMS.

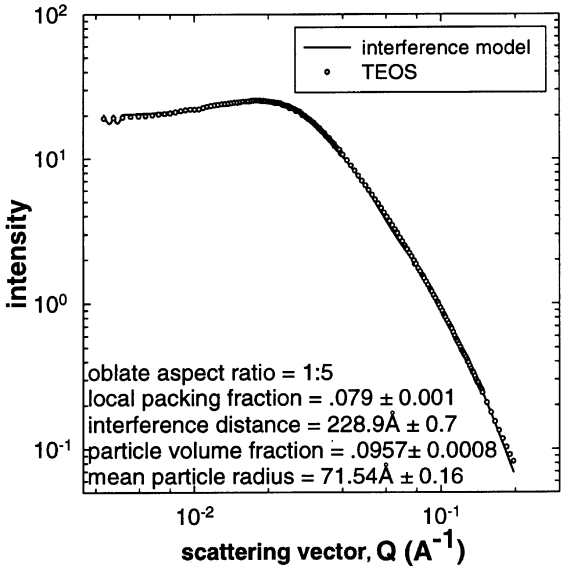

Fig. 2. Interference model fit of based-catalyzed TEOS standard deviations of $I(Q)$ are <2% for $Q < 0.3$ and <7% for $Q > 0.3$.

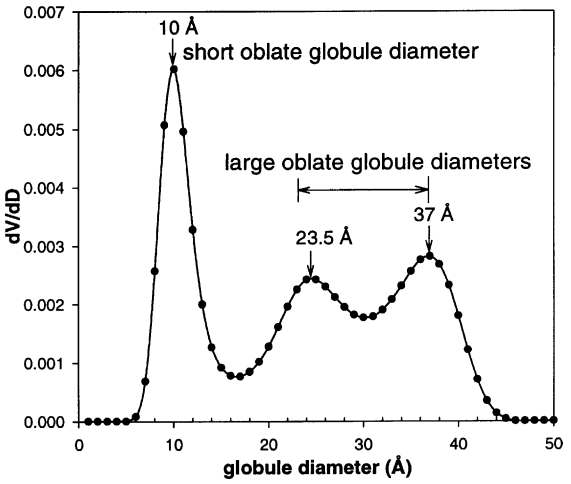

Fig. 3. Maximum entropy fit of high Q data of base-catalyzed TEOS.

behavior is not apparent in an aerogel, these elements can be removed from modeling.

SANS results for the TES samples appeared to demonstrate mass fractal behavior (Fig. 4). The fractal models of the TES samples showed nearly identical behavior and supported a volume or

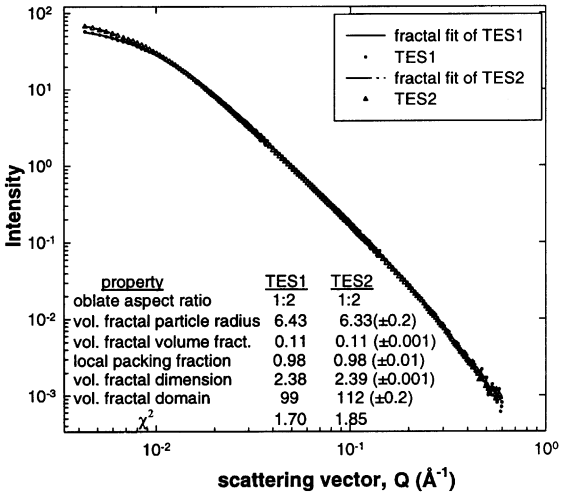

Fig. 4. Fractal model fit of two TES samples, standard deviations of $I(Q)$ are <2% for $Q < 0.3$ and <7% for $0.3 < Q < 0.45$ and >10% for $Q > 0.45$.

mass fractal structure with a local packing fraction of nearly unity. The mass fractal dimensions are about 2.4, and the mass fractal domains (or correlation length) range between 100 and 110 Å.

The fractal modeling of the scattering data for TMS required surface fractal contributions to produce a good fit. The region of a slightly steeper non-integral slope in the SANS results also suggests a surface fractal contribution. In Fig. 5, the details of the model indicate that the volume fractal correlation lengths are much smaller than for TES, the globules are more oblate, and the surface fractal domains are about 83 Å.

In each case, exhaustive attempts were made to fit spherical and prolate globules to the scattering data; however, neither of these structures reasonably fit the data. Following the failure of the other globule geometries, oblate particles successfully fit the results. While unexpected, oblate structures are possible considering the propensity of silica to form three and four-membered rings [17], and planar sheets [18], and plate-like aggregates [19].

4. Discussion

This TEOS sample was base-catalyzed (pH = 9.6), and therefore, synthesized under rel-

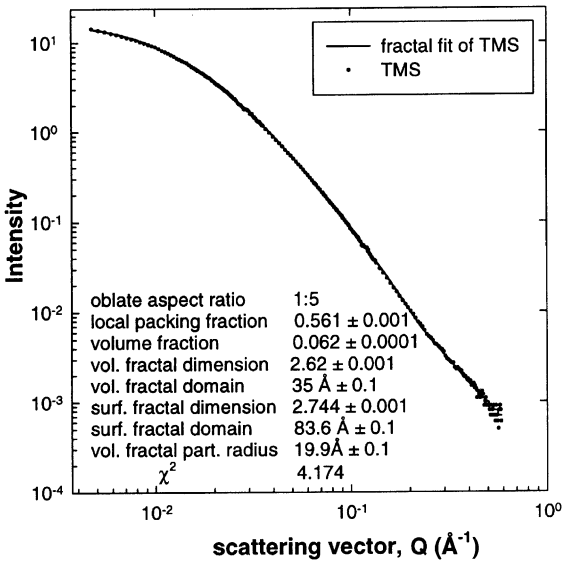

Fig. 5. Fractal model fit of TMS including volume and surface fractal components, standard deviations of $I(Q)$ are <2% for $Q < 0.25$ and <7% for $0.25 < Q < 0.43$ and >10% for $Q > 0.43$.

atively rapid condensation rates and slower hydrolysis rates. From these conditions, one might expect a densely packed agglomerated colloidal structure. The interference model results support particle structure; however, the particles seem to be very loosely packed. The very small length scale structures (10 Å) described by the maximum entropy model may be similar to ringed-oligomer building blocks reported by Engelhardt et al. in aqueous silicate solutions [20]. Although alkoxide/alcohol/water solutions are less likely to form these rings at high pH than aqueous solutions, the length scales suggested by the maximum entropy model indicate that such reactions are possible. Because ring formation reactions are not favored at lower pHs, future SANS experiments and maximum entropy modeling will include samples synthesized under several pH values to observe changes in small length scale structures.

The TEOS interference and maximum entropy models suggest a consistent particle structure. The interference mean radius and oblate aspect ratio data indicate meso-sized particles – 142 Å × 28 Å. The short diameter coincides with the average nanoparticle long diameter (30 Å) described by the maximum entropy model. The oblate meso-particle may be comprised of the oblate (30 Å × 10 Å) nanoparticles.

TES and TMS derived aerogels have three alkoxide groups and a hydrogen bonded to the silicon atom. The absence of an alkoxide (and/or the presence of a hydrogen) effect the partial charge on the silicon, and, consequently, the reactivities of these compounds differ from the tetra-alkoxide TEOS. TES and TMS form gels much more rapidly than TEOS, and without the need of a catalyst. Because the synthesis reactions for TES and TMS occur more rapidly and at a lower pH (pH $\sim$ 5), decidedly different structures were expected than observed in TEOS. The lower pH during synthesis suggested that condensation would be irreversible preventing restructuring processes and creating open randomly branched structures [21]. Based on these assertions, these data were modeled ignoring surface fractal behavior. To check our conjectures, we also modeled with surface fractal contributions, but analysis without surface fractal behavior provided a superior fit.

TMS physically differs from TES only in the size of its alkoxide groups; however, attempts to exclude surface fractal elements during modeling rendered unacceptable fits. Introduction of surface fractal contributions provided reliable fitting, but the resulting model described a microstructure quite different from TES (Fig. 5). Visual inspection of the respective SANS plots in Fig. 2 suggests two different material morphologies. The TMS aerogel is not as densely packed (local packing fraction = 0.56), and its particles are more oblate (aspect ratio = 1/5). These differences in structure could be due to the more rapid gelation of TMS.

While noting that limitations exist in the modeling of scattering data because alternative interpretations of results are often possible, the particular data presented here provided some striking findings. Oblate structures were not expected from these results; spherical or prolate structures seemed much more likely. However, these models were unable to provide reasonable fits using either spheres or prolate structures but fitted readily when an oblate particle shape was

assumed. It is well known that the scattering from a dilute concentration of polydispersed spheroids is not sensitive to the spheroid aspect ratio, but the situation is different when interference effects are evident. The presence of an interference peak in the present TEOS scattering data points to a narrow particle size distribution (whether exactly lognormal or not) and also a relatively narrow distribution of nearest-neighbor (interference) distances. For an interconnected system as assumed here, the relationship between the interference-distance distribution implicit in the model and the particle size distribution can be strongly affected by the particle shape. Using the oblate shapes found to give satisfactory fits, the present model gives a typical interference distance, D_{int}, of 228 Å while the typical mean oblate particle diameter, $2R_{\text{o}}$, is 142 Å for the TEOS system. Thus, this physical model of the structure strongly suggests an interconnected assembly of unstacked oblate particles, rather than the network of prolate 'strut'-like particles assumed initially.

5. Conclusions

Analysis of SANS results using interference, maximum entropy and fractal models may be a significant characterization tool for aerogel structures. The three model aerogels were chosen because of their differences in structure, and the models provided detailed structural descriptions over a wide range of length scales. Analysis of the TEOS aerogel using interference and maximum entropy models indicated an arrangement of regularly-spaced oblate meso-sized particles comprised of oblate nanoparticles. Employing the fractal model, the TES and TMS samples showed volume fractal and volume and surface fractal behavior, respectively. The differences in structure may be attributed to the respective kinetics of gelation. Confirmation of these structural interpretations is currently being sought through transmission electron microscopy and gas adsorption methods.

Acknowledgements

The authors wish to thank the Center for Neutron Research at the National Institute of Standards and Technology and NSF for access to the NG-7 neutron beam line.

References

[1] G.G. Long, S. Krueger, P.R. Jemian, D.R. Black, H.E. Burdette, J.P. Cline, R.A. Gerhardt, J. Appl. Crystallogr. 23 (1990) 535.
[2] D.W. Hua, J. Anderson, S. Haereid, D.M. Smith, G. Beaucage, Mater. Res. Soc. Sympos. 346 (1994) 985.
[3] J. Wang, J. Shen, B. Zhou, X. Wu, Nanostructured Mater. 7,6 (1996) 699.
[4] D.W. Schaeffer, C.J. Brinker, J.P. Wilcoxon, D.Q. Wu, J.C. Phillips, B. Chu, Mater. Res. Soc. Sympos. 121 (1988) 691.
[5] A.B. Jarzebski, J. Lorenc, L. Pajak, Langmuir 13 (1997) 1280.
[6] J. Mrowiec-Bialon, L. Pajak, A.B. Jarzebski, A.I. Lachowski, J.J. Malinowski, Langmuir 13 (1997) 6310.
[7] J. Hyeon-Lee, G. Beaucage, S.E. Prantsinis, S. Vemury, Langmuir 14 (1998) 5751.
[8] G. Beaucage, D.W. Schaefer, J. Non-Cryst. Solids 172–174 (1994) 797.
[9] G. Beaucage, J. Appl. Crystallogr. 28 (1995) 717.
[10] A.J. Allen, S. Krueger, G. Skandan, G.G. Long, H. Hahn, H.M. Kerch, J.C. Parker, M.N. Ali, J. Am. Ceram. Soc. 79 (5) (1996) 1201.
[11] A.J. Allen, R.A. Livingston, in: V.M. Malhotra (Ed.), Fifth International Conference on Fly Ash, Silica Fume, Slag and Natural Pozzolans in Concrete, American Concrete Institute, 1995.
[12] A.J. Allen, J. Appl. Crystallogr. 24 (1991) 624.
[13] W.L. Griffith, R. Triolo, A.L. Cooper, Phys. Rev. A 35 (1987) 2200.
[14] M. Kotlarchyk, S.H. Chen, J. Chem. Phys. 79 (1983) 2461.
[15] J.A. Potton, G.J. Daniell, B.D. Rainford, J. Appl. Crystallogr. 21 (1988) 663.
[16] A.J. Allen, R.A. Livingston, Adv. Cem. Based Mater. 8 (1998) 118.
[17] J.L. Coffer, T.W. Zerda, K.J. Taylor, S. Martin, Mater. Res. Soc. Sympos. Proc. 612, D.5.10.1, 2000.
[18] R.K. Iler, The Chemistry of Silica, Wiley, New York, 1979, p. 388.
[19] C.J. Brinker, G.W. Scherer, Sol–Gel Science – The Physics and Chemistry of Sol–Gel Processing, Academic Press, San Diego, CA, 1990, p. 261.
[20] V. Engelhardt, W. Altenberg, D. Hoebbel, W. Wieker, Anorg. Allg. Chem. 418 (1997) 43.
[21] C.J. Brinker, G.W. Scherer, Sol–Gel Science – The Physics and Chemistry of Sol–Gel Processing, Academic Press, San Diego, CA, 1990, p. 203.